Droplet Impact Behavior on Convex Surfaces with a Circumferential Wettability Difference

Taku Ishikawa[1], *Yutaka Yamada*[*2], *Kazuma Isobe*[2], *Akihiko Horibe*[2]

[1]Graduate School of Environmental, Life, Natural Science and Technology, Okayama University, Kita-ku, Okayama 700-8530, Japan

[2]Faculty of Environmental, Life, Natural Science and Technology, Okayama University, Kita-ku, Okayama 700-8530, Japan

Author information

*Corresponding author

Yutaka Yamada

Tel.: +81 86 251 8046. E-mail: y.yamada@okayama-u.ac.jp

ORCID

Yutaka Yamada: 0000-0002-2823-6790

ABSTRACT

Controlling the bouncing behavior of the impacting droplets is an important issue for splay cooling, icing prevention, and other applications. The bouncing behavior of impacting droplets on superhydrophobic curved surfaces and flat substrates with a wettability difference has been widely investigated, and droplets impacting these surfaces show shorter contact times than on superhydrophobic flat surfaces and droplet transport. However, there have been few studies on the droplet impact behavior on curved surfaces with a wettability difference, where efficient droplet control could be achieved by combining the features. In the present study, droplet impact experiments were conducted using copper cylinders with different circumferential wettability from hydrophilic to superhydrophobic, varying the impact velocity, cylinder diameter, and rotation angle. Droplets that impacted the wettability boundary showed asymmetric deformation and moved to the hydrophilic side owing to the driving force of the wettability difference. Moreover, the droplet behavior was classified into four types: the droplet bounced off the surface, the droplet bounced off the surface and split, the droplet attached to the surface, and the droplet attached to the surface and split. The droplet behavior was estimated using the maximum spreading width of the droplet impacted on the flat substrate. We evaluated whether the droplets attached to the surface or bounced off the surface after impact using the Weber number and rotation angle, and the estimations were in agreement with the experiment results for the cylinder diameter of 4 and 6 mm.

INTRODUCTION

The impact of droplets on solid surfaces is observed in daily life, such as rain droplets impacting surfaces, and in industrial applications, such as in inkjet printing, spray cooling, prevention of icing on aircraft wings, and self-cleaning of walls.[1–5] Therefore, understanding the droplet impact behavior is crucial for improving these applications. In general, this impact phenomenon is dependent on factors such as the surface free energy of the solid surface and droplet, the surface structure of the solid substrate, and the velocity of the droplet.[6–9] Based on these factors, previous studies have attempted to understand the dynamics of the droplet impact phenomenon and improve such applications.[10–18] For example, reduction of the contact time between the droplet and solid surface has been investigated in various fields, such as self-cleaning surfaces and freezing caused by droplet adhesion. Liu et al.[19] performed droplet impact experiments using superhydrophobic flat substrates with different microstructure geometries. They found that a difference in the capillary force induces a difference in the droplet bounce behavior, which can reduce the contact time of the droplet on the surface.

In recent years, droplet impact experiments on curved surfaces have been conducted to gain a better understanding of the wetting phenomena during inkjet printing on curved surfaces and ice protection of pipes.[20–24] Although curved surfaces include both concave and convex surfaces, convex surfaces have attracted more attention because they have many possibilities for controlling the impact behavior of droplets. For example, Liu et al.[25] experimentally and numerically studied the droplet impact on a superhydrophobic surface with curvature larger than the droplet diameter. The contact

time on the curved surface was approximately 40% less than that on the flat substrate. The asymmetricity of the circumferential and axial momentum and the mass distribution of the droplet after impact affect the contact time. Andrew et al.[26] focused on the ratio of the droplet diameter to the solid cylinder diameter. They found that the contact time of the droplet varies with the diameter ratio, and it is minimized when these diameters are comparable. Yin et al.[27] performed droplet impact experiments using wires with diameters smaller than the droplet diameter and classified the droplet splitting behavior.

The results of droplet impact experiments on convex surfaces suggest that it is possible to control the contact time and number of split droplets.[25–27] However, it is difficult to precisely control the behavior of droplets after bouncing because the behavior of the droplets sensitively depends on the very small differences in the landing positions on the convex surface. Consequently, droplet control using only superhydrophobic convex surfaces has limitations. Therefore, to achieve directional droplet transport by bouncing, flat substrates with a wettability difference have been studied.[28–32] This property can be achieved by altering the structure and chemical properties of the surface. Subramanian et al.[33] studied the motion of droplets on surfaces with wettability gradients and revealed the motion of the droplets in the hydrophilic direction. Chu et al.[34] studied substrates with step-like wettability differences ranging from superhydrophobic to hydrophilic. They found that when a droplet impacted the wettability boundary, the droplet asymmetrically spread and then bounced back toward the more hydrophilic side. This indicates the possibility of directional droplet bouncing by varying the distance from the wettability boundary to the droplet center axis at the

moment of impact. Wang et al. simulated the impact behavior of two droplets on a flat substrate with a wettability difference, and it was confirmed that the contact time varies depending on the strength of the wettability difference, Weber number, and the distance between droplets.[35]

Studies focusing on reducing the contact time and droplet transport to maintain a clean and dry solid surface have been performed on three major types of surfaces: superhydrophobic flat substrates, superhydrophobic convex surfaces, and flat substrates with wettability difference. However, a curved surface with a wettability difference will achieve more accurate droplet control by the contact time reduction and droplet transport which are potentially applied for ice prevention, self-cleaning surfaces, and direction control of bouncing droplet by varying surface curvature.

In this study, we focused on cylinders with a wettability difference in the circumferential direction. The results showed asymmetrical spreading of the three-phase contact line of the droplet at the wettability boundary. Splitting, attachment, and rebounding of the droplet were observed after the impact, and we evaluated whether the droplet attached to or bounced off the surface based on the relationship between the Weber number and rotation angle of the cylinder.

EXPERIMENTAL METHODS

Sample Preparation. Cylindrical copper rods with diameter (D_c) ranging from 1 to 6 mm and length of 20 mm were used as samples. The samples were polished with abrasive papers (#1000 and #2000), ultrasonically cleaned in ethanol (Fujifilm Wako Pure Chemical Co., Osaka, Japan) for 15 minutes, rinsed with purified water (CPW-102, Advantec Toyo Kaisha, Ltd., Tokyo, Japan), and

dried under a stream of compressed air. They were then immersed in 6 M hydrochloric acid solution for 30 s to remove the oxide layer from the sample surfaces, followed by rinsing and drying. The samples were then dipped in 2.5 M sodium hydroxide (NaOH, Fujifilm Wako Pure Chemical Co.) and 0.1 M ammonium peroxydisulfate ($(NH_4)_2S_2O_8$, Fujifilm Wako Pure Chemical Co.) at 4 °C for 1 h to fabricate nanostructures on the cylinder surface, followed by rinsing and drying. The samples were subsequently immersed in a solution consisting of 1*H*,1*H*,2*H*,2*H*-perfluorooctyltriethoxysilane ($C_{14}H_{19}F_{13}O_3Si$, Sigma Aldrich Co. St. Louis, MO, USA), water, and ethanol (at a volume ratio of 1:1:100) for 3 h to make the surface superhydrophobic. The samples were then rinsed with ethanol and water, dried, and stored at room temperature for 3 h. Finally, a thin gold film was deposited on one side of the cylinder with an ion coater (IB-3, Eiko Co., Tokyo, Japan) operated with an ionic current of 4 mA for 8 min to make a hydrophilic surface. In addition, we prepared a flat substrate by the same procedure for comparison.

Sample Characterization. The surface structures of the cylinder were characterized by scanning electron microscopy (SEM, JEOL7001F, JEOL Co., Tokyo, Japan). The accelerating voltage was set to 10 kV.

The static contact angle of each surface θ was measured by the sessile droplet method. To measure the contact angle, a purified water droplet with a volume of 3.5 μL was gently deposited on the surface, and the droplet shape was captured by a high-speed camera (Cyclone-1HS-3500-C, Optronis Co., Kehl, Germany). Dynamic contact angles (advancing contact angle θ_a and receding contact angle θ_r) were measured using the expansion-contraction method. For the advancing contact

angle, 3.5 μL of water was dropped on the substrate using a syringe pump (YSP-201, YMC Co., Kyoto, Japan), to which additional liquid was added to expand the droplet and advance the interface. For the receding contact angle, water was dropped on the substrate in the same way, and then the droplet was contracted by sucking up the liquid with a syringe. The movement of the three-phase contact line was captured by a high-speed camera and both angles were measured.

Droplet Impact Experiments. The setup for the droplet impact experiments is shown in Figure 1(a). A water droplet was dropped on the copper cylinder from a syringe above the copper cylinder. The droplet impact velocity (v) was changed from 0.2 m/s to 2.0 m/s by adjusting the height of the syringe above the copper cylinder. To avoid displacement of the droplet from the center of the cylinder during the impingement process, the path of the droplet was covered by an acrylic pipe to 20 mm above the sample. The droplet impact process was recorded from the azimuthal direction of the cylinder by the same high-speed camera as that used for recording the droplet shape with a frame rate of 5000 fps. All of the droplet impact experiments were performed at 20.5 ± 1.0 °C and 52% ± 10% relative humidity. The experiment was conducted three times for each condition and the same impact behavior was observed at each condition. The error in the impact velocity was less than 5%.

The droplet impact experiments and contact angle measurements were conducted by rotating the copper cylinder. The wettability boundary was used to define the rotation angle, as shown in Figure 1(b). Here, the cylinder was rotated counterclockwise, and the angle formed by the boundary, cylinder center, and horizontal axis was defined as the rotation angle ϕ. Accordingly, $\phi = 90°$ means that the wettability boundary coincides with the vertical axis of the cylinder, and the left- and right-

hand sides of the cylinder show hydrophilic and superhydrophobic characteristics, respectively.

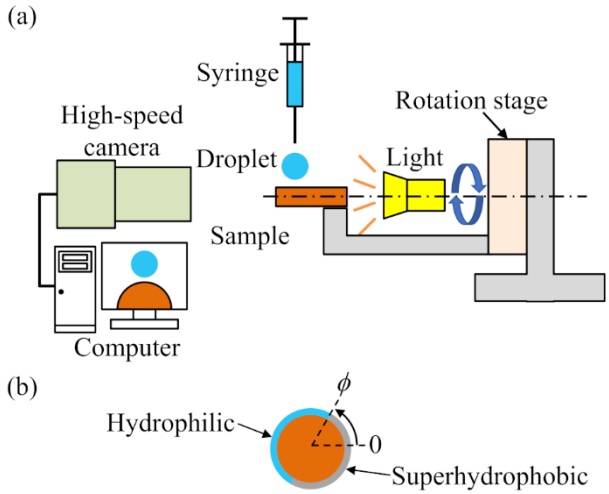

Figure 1. (a) Experimental setup. (b) Definition of the rotation angle ϕ.

RESULTS AND DISCUSSION

Surface Characterization. A SEM image of the flat copper substrate is shown in Figure 2(a). Needle-like structures with a diameter of 0.3 μm and lengths of several micrometers were randomly distributed on the surface. This was caused by the chemical etching of the surface through the chemical reaction[36]

$$Cu + 4OH^- + (NH_4)_2S_2O_8 \rightarrow Cu(OH)_2 + 2SO_4^{2-} + 2NH_3 + 2H_2O \quad (1)$$

during immersion of the substrate in the aqueous solution of sodium hydroxide and ammonium peroxydisulfate.

The results of the contact angle measurements for the cylinder with a diameter of 6 mm are shown in Figure 2(b). The static contact angles were 18±2°, 12±3°, and 17±3° for ϕ = 0°, 30°, and 60°, respectively, and accordingly, these regions are hydrophilic. The droplet deposited at ϕ = 120°–180° immediately rolled off instead of to attach on the cylinder. Accordingly, the contact angle at

1 these regions could not measure at this experiment, and thus θ was plotted as 180°. As a reference
2 value, the contact angle of the flat copper substrate modified by same procedure was estimated to be
3 153±3° (see the insert in Figure 2(b)) The difference in contact angle between the hydrophilic and
4 superhydrophobic flat substrates was more than 130°. In addition, the dynamic contact angles of the
5 superhydrophobic substrate were 159±3° and 152±2° for the advancing and receding contact angles.
6 At ϕ = 90°, the droplet was deposited on the cylinder with the hydrophilic surface on the left-hand
7 side and the superhydrophobic surface on the right-hand side. As a result, the droplet moved toward
8 the hydrophilic side, as shown in Figure 2(c). The time t is the time since the droplet contacted the
9 solid surface. The movement of the droplet toward the hydrophilic side is caused by the force
10 generated by the existence of a static contact angle difference between the two sides of the droplet.
11 This force can be estimated by[37]

12 $$dF = \gamma_{\mathrm{LV}}(\cos\theta_{\mathrm{A}} - \cos\theta_{\mathrm{B}})dx \qquad (2)$$

13 where γ_{LV} is the surface tension between the liquid and gas phases, and θ_{A} and θ_{B} are the static
14 contact angles, where $\theta_{\mathrm{A}} < \theta_{\mathrm{B}}$. This equation indicates that the wettability difference generates a force
15 to induce the droplet to move toward the hydrophilic side of the cylinder.

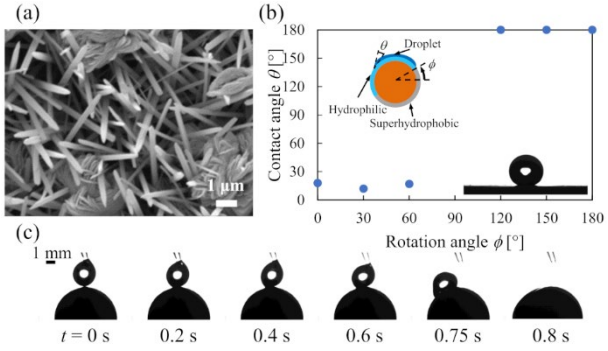

16

Figure 2. (a) SEM image of the nanostructure of the flat substrate. (b) Relationship between the rotation angle ϕ and static contact angle θ. The insert shows a droplet on the superhydrophobic flat substrate. (c) Behavior of the droplet deposited on the cylinder with a wettability difference at ϕ = 90°.

Droplet Impact Experiments. Although the flat substrate is a fundamental structure, many curved surfaces are observed in artificial structures. It is important to understand the impact behavior of droplets on curved surfaces, such as airplane wings, car bodies, and pipes, because droplets often impact these surfaces. In addition, a wettability difference on the solid surface enables droplet movement, which is expected to have industrial applications. Therefore, we conducted experiments to investigate the effects of the rotation angle, impact velocity, and diameter of the cylinder on the droplet impact behavior using cylinders with a wettability difference in the circumferential direction. The droplet impact behavior on the cylinder with a diameter of 6 mm at an impact velocity of 0.5 m/s and rotation angles of ϕ = 0°, 90°, and 180° is shown in Figure 3 (movies of the droplet behavior are provided in the Supporting Information, Movies 1–3). At ϕ = 0°, the droplet spread after impact because the contact area only showed the hydrophilic characteristic, and the three-phase contact line showed no contraction. At ϕ = 180°, the droplet deformed to a pancake-like shape after impact, and then the three-phase contact line receded. Finally, the droplet completely bounced off the cylinder because the contact area only showed the superhydrophobic characteristic. In these two cases, the droplet exhibited symmetric behavior owing to the uniform wettability of the solid–liquid interface. However, asymmetric behavior was observed at ϕ = 90°. In particular, the part of the droplet

impacting the superhydrophobic half of the cylinder bounced off the cylinder, while that impacting the hydrophilic half spread on the cylinder. Subsequently, the right-hand side of the droplet moved toward the hydrophilic side because of the wettability difference.

The movement of the three-phase contact line after droplet impact as a function of time is shown in Figure 4(a). Here, as shown in Figure 4(b), ϕ_R and ϕ_L ,which are defined as the angle between the three-phase contact line and the cylinder top, are used for the evaluation. At $\phi = 0°$, the droplet spread and reached to ϕ_R=81° and ϕ_L =-83°, completely covering the hydrophilic region where the gold film was deposited. At $\phi = 180°$, the three-phase contact line expanded until approximately 4 ms after impact owing to the inertial force, and it then receded and completely bounced off the cylinder within 10.4 ms. The droplet then fell onto the cylinder owing to gravity and impacted it again at approximately 50 ms, eventually sliding off the solid surface. The results for $\phi = 90°$ showed that the behavior of the right-hand side of the droplet coincided with the results at $\phi = 180°$ until t =10 ms, while the behavior of the left-hand side of the droplet was similar to that at $\phi = 0°$. This is because of the wettability difference in the contact area, which affects the transition of the three-phase contact line. This mechanism can be explained by the work of adhesion W_{SL}, which is influenced by the wettability of the solid surface. The work of adhesion per unit area is defined as

$$W_{SL} = \gamma_{SV} + \gamma_{LV} - \gamma_{SL} = \gamma_{LV}(1 + \cos\theta) \quad (3)$$

Where γ_{SV} is the interfacial tension between the solid and gas phases, and γ_{SL} is the interfacial tension between the solid and liquid phases. The work of adhesion is the energy required to detach from the substrate and form new solid–gas and liquid–gas interfaces. From this equation, the work of adhesion

depends on the contact angle, and the work of adhesion is larger on the hydrophilic side of the cylinder than on the hydrophobic side of the cylinder. As a result, the difference in the work of adhesion between the left- and right-hand sides induces asymmetric behavior after impact at $\phi = 90°$.

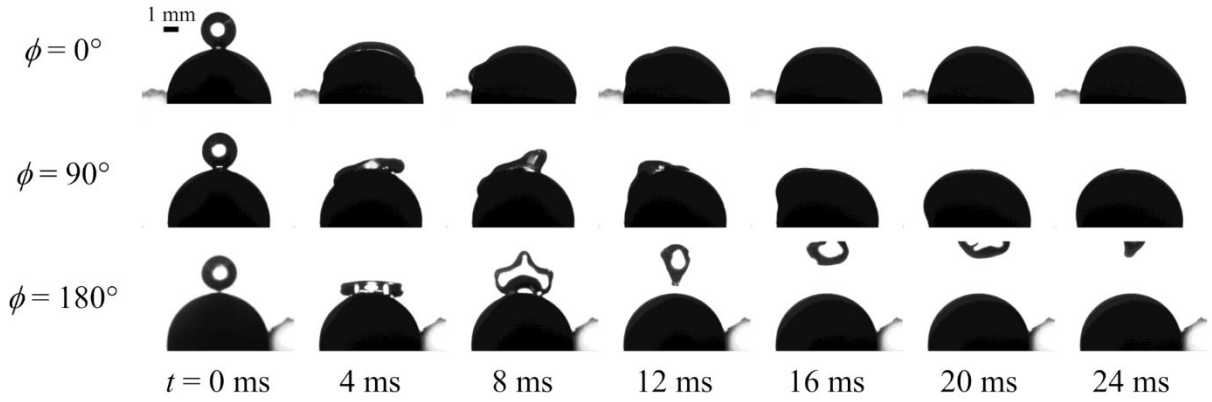

Figure 3. Snapshots of the droplet impact on the cylinder with a diameter of 6 mm at an impact velocity (v) of 0.5 m/s.

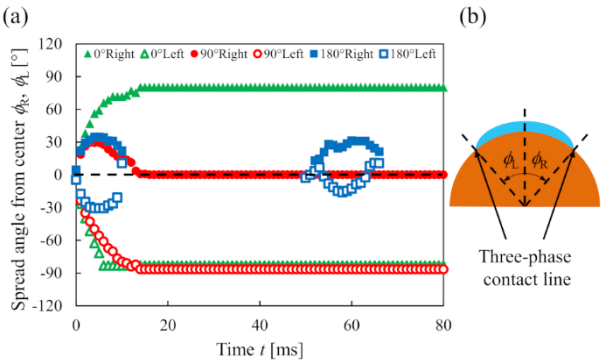

Figure 4. (a) Transition of the three-phase contact line. (b) Definition of the spread angle from the center axis of the cylinder.

Effect of the Impact Velocity. Snapshots of the impact behavior on the cylinder with a diameter of 6 mm at impact velocities of 0.2 and 1.5 m/s at $\phi = 90°$ are shown in Figure 5 (movies of the droplet behavior are provided in the Supporting Information, Movies 4 and 5). The droplet spread

to both sides of the cylinder after impact. It then moved to the hydrophilic side owing to the wettability difference at 0.2 m/s, which was similar behavior to that at v = 0.5 m/s. At v = 1.5 m/s, the right-hand side of the droplet spread on the superhydrophobic surface, and it began to detach from the surface at approximately 6 ms. The droplet then split at the wettability boundary located at the top of the cylinder after approximately 8 ms. This droplet further split into multiple droplets in air. The number of split droplets tended to increase with the impact velocity of the droplet while the volume of each split droplets decreased. On the other hand, the droplets on the hydrophilic side of the cylinder remained on the solid surface. The results of droplets breaking up and bouncing off at the wettability boundary are similar to the results of the study conducted by Chu et al. in which impact experiments were carried out on the substrate with wettability difference. [34] In their study, they confirmed that droplets adhered to the hydrophilic region, split into droplets by bouncing off, and the resulting droplets flew in the hydrophilic direction. However, in our experiment, it was found that the rebound direction was different, and the droplet rebounded in the superhydrophobic direction.

The transition of the three-phase contact line with time is shown in Figure 6. The definition of the three-phase contact line location is shown in Figure 4(b). At v = 0.2 m/s, the three-phase contact line at the right-hand side gradually moved to the hydrophilic side during the retreating motion. Conversely, at v = 1.5 m/s, the right three-phase contact line spread until 5 ms and then abruptly changed from ϕ_R=80° to 0°. This is because the droplets in contact with the superhydrophobic part of the cylinder bounced back at 5.8 ms, and therefore the three-phase contact line receded to the hydrophilic region. Here, the Weber number $We = \rho D v^2/\gamma_{LV}$, where ρ is the density, D is the droplet

diameter before impact, and v is the impact velocity, is introduced to discuss the droplet behavior. Because We = 1.1 at v = 0.2 m/s, the inertial force was comparable with the surface tension, and the droplet remained as a single droplet even though it was deformed by the impact and the wettability difference. Conversely, We = 62 at v = 1.5 m/s, and the inertial force of the droplet that promotes the deformation was significantly greater than the surface tension. As a result, the droplet split into several small droplets.

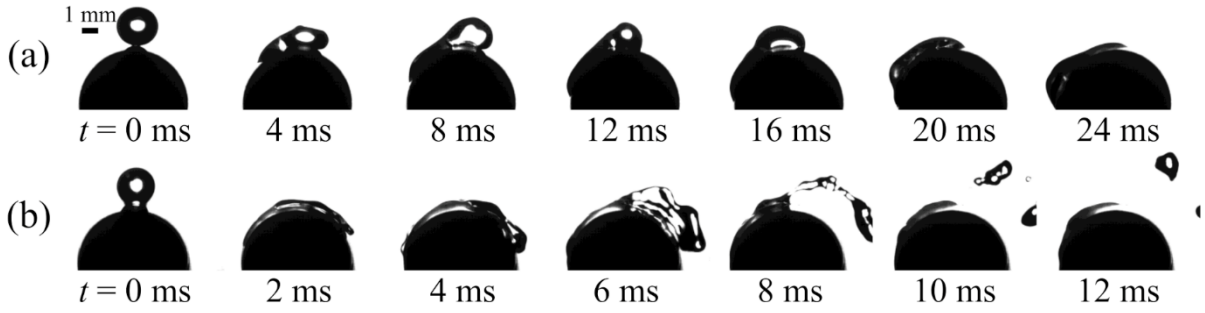

Figure 5. Snapshots of the droplet impact on the cylinder with a diameter 6 mm for impact velocities of (a) 0.2 and (b) 1.5 m/s.

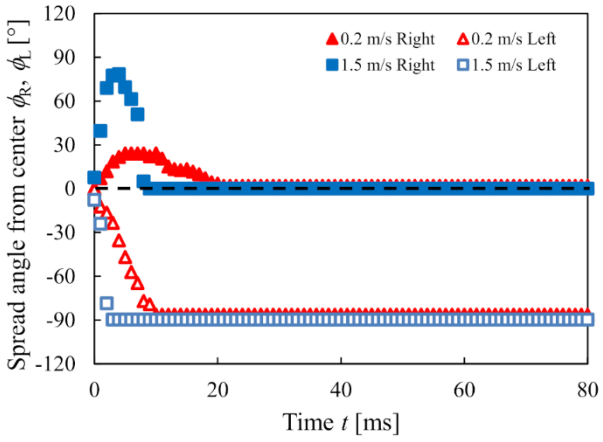

Figure 6. Transition of the three-phase contact line as a function of time for impact velocities of 0.2 and 1.5 m/s.

Effect of the Cylinder Diameter. We also investigated the effect of the curvature of the solid surface on the impact behavior by changing the diameter of the cylinder. The impact behavior for cylinders with diameters of 1, 2, and 4 mm is shown in Figure 7. The rotation angle and impact velocity were set to 90° and 0.5 m/s, respectively (movies of the droplet behavior are provided in the Supporting Information, Movies 6–8). Droplet splitting was observed for all of the samples, except for the cylinder with a diameter of 6 mm (Figure 3). The droplet more easily split as the cylinder diameter decreased. This is considered to be because of the energy balance of the droplet. In the flat substrate case, the inertial energy of the impacted droplet is converted to surface free energy and viscous dissipation during the deformation.[38] However, although some of the inertial energy was converted into surface free energy and viscous dissipation, certain inertial energy remained because the droplet spread along the circumferential direction of the cylinder. As a result, the droplet broke up without retraction motion. In addition, for the cylinders with diameters of 1 and 2 mm, the droplet was observed to attach to the entire hydrophilic area within 8 ms.

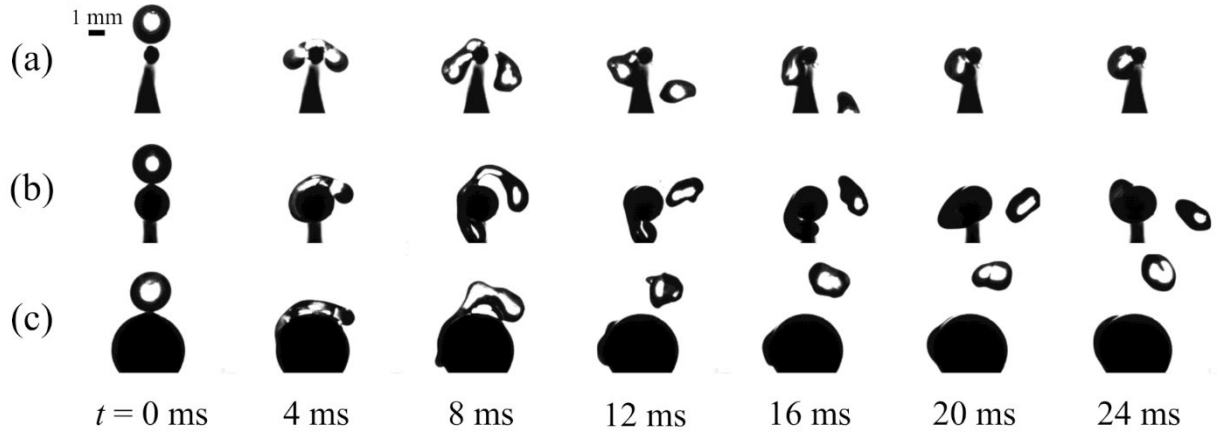

Figure 7. Snapshots of the droplet impact on the cylinder at v = 0.5 m/s for cylinder diameters of (a)

1, (b) 2, and (c) 4 mm.

We also evaluated the contact time of the droplet under the conditions of D_c = 2, 4, and 6 mm, ϕ=180°, and v = 0.5 m/s, where no droplets attached to the surface, because the contact behavior is important for the droplet behavior. The contact times for D_c = 2, 4, and 6 mm were 8.0, 8.4, and 10.2 ms, respectively, and the contact time for the flat substrate was 10.4 ms. In a previous study, Liu et al.[25] reported that when a droplet impacts a curved surface, the axial contraction is faster and the contact time is shorter compared with those on a flat surface. Using their formula for estimating the contact time to a curved surface, the contact times for diameters of 2,4 and 6 mm were estimated to be 7.4, 8.5, and 10.8 ms, respectively. The relation between the contact time and the cylinder diameter shows good agreement with our results.

The present results showed that the impact behavior of a droplet on a cylinder depends on the wettability of the cylinder, cylinder diameter, and impact velocity of the droplet. To summarize the results, the droplet impact behavior under each set of conditions was classified into four categories: (I) the droplet bounced off the surface, (II) the droplet bounced off the surface and split, (III) the droplet attached to the surface, and (IV) the droplet attached to the surface and split (Figure 8). For comparison, Figure 8(e) shows the results for the flat substrate with a wettability difference. The position of the impact is defined as shown in Figure 8(f), where x=0 mm is the wettability boundary, and the superhydrophobic side is positive. There were three major trends: (i) the droplet tended to split at high impact velocity, (ii)the angle at which the lowest impact velocity for droplet splitting was ϕ = 120° for D_c = 2-6 mm, and (iii) the droplet more easily attached to the cylinder for

smaller D_c. For (i), at v = 2.0 m/s, the droplets split for all D_c at $\phi \geq 30°$. However, at v = 0.2 m/s, the droplet only split for D_c = 1 mm at $\phi = 180°$. As described in the previous section, the reason for this tendency is that the inertial energy of the droplet after impact becomes larger for increasing impact velocity, and the droplet cannot maintain a single droplet shape. For (ii), at $\phi = 120°$, the left end of the droplet reached the hydrophilic region, while the rest of the droplet was on the superhydrophobic part and bounced back. This behavior is similar to $\phi = 90°$, but at $\phi = 120°$, a larger part of the droplet tends to bounce off and a smaller part remains on the hydrophilic region. Therefore, the bouncing part tends to be dominant rather than the remaining part. This behavior is more likely to occur than at $\phi = 90°$, and as a result, the splitting occurred even at low velocity. For (iii), droplet attachment to the cylinder occurred under all conditions for D_c = 1 mm. For D_c = 2–6 mm, droplet bouncing was observed when the impact velocity was small and the rotation angle was large, and droplet attachment occurred at all velocities for $\phi \leq 90°$. For D_c = 4 and 6 mm, the droplet did not attach to the cylinder even for v = 2.0 m/s at $\phi = 180°$, because the upper part of the cylinder was not hydrophilic. However, for D_c = 1 and 2 mm, the impacted droplet spread around to the lower surface and wetted the hydrophilic part of the cylinder, resulting in attachment to the hydrophilic part of the cylinder.

To understand the impact behavior on the cylinders with different wettability, we estimated the conditions at which droplet attachment occurs. Here, the maximum spreading width D_{max} has the following relation with We:[39]

$$D_{\max} \sim D_o We^{1/4} \tag{4}$$

In the present study, this relation was confirmed by measuring the maximum spreading widths of the

droplets impacting the superhydrophobic flat substrate at v = 0.2–2.0 m/s, and it was fitted with a coefficient of 1.02. This equation was used to estimate the three-phase contact line location to determine whether the three-phase contact line reached the wettability boundary. Although the actual location of the three-phase contact line is overestimated by equation (4) owing to the shape of the spreading droplet, the difference is assumed to be small. According to this assumption, the width of the three-phase contact line at the maximum spreading L_{max} shown in Figure 9 (a) is assumed to be comparable with D_{max}. Comparing D_{max} of the superhydrophobic substrate with L_{max} of the cylinder with D_c = 6 mm at ϕ = 180° and v = 0.5 m/s, the ratio is estimated to be D_{max}/L_{max} = 1.03. Considering the threshold for the attachment of the droplet to the hydrophilic part of the cylinder, attachment to the cylinder depends on whether the left-hand side of the droplet touches the hydrophilic part of the cylinder. Therefore, the position of the left-hand side of the droplet at the maximum spreading was converted to the counterclockwise angle from the horizontal axis ϕ_e, as shown in Figure 9 (a). Similarly, Figure 9(b) shows a schematic diagram of the half of the maximum spreading width of the droplet and the off-center distance from the wettability boundary at the flat substrate.

The predicted left three-phase contact line location of the droplet at the maximum spreading angle ϕ_e or $D_{max}/2$ at each *We* is shown as a solid line in Figure 8(a)–(e). A larger rotation angle than the estimated angle ϕ_e or larger off-center distance x than the half of the D_{max} indicate that the contact area of the droplet is only on the superhydrophobic region and, accordingly, the droplet is expected to bounce off the cylinder. The trend of the predicted results showed agreement with the experimental

results at D_c= 4, 6 mm and the flat substrate. However, for part of D_c = 2 and 4 mm, the droplet bounced even though the rotation angle was less than the estimated angle ϕ_e. This was caused by the conversion to the angle ϕ_e. The droplet impacting the cylinder with a diameter of 4 mm at ϕ = 180° is shown in Figure 10(a). The discrepancy between the three-phase contact line and the maximum spreading width is small in terms of the distance. However, when this discrepancy is converted to the circumferential angle difference $\Delta\phi$, the discrepancy becomes relatively large because D_c is small. In addition, the impact velocity and cylinder diameter are considered to affect the estimated maximum spreading width. The relationships between the ratio of the initial droplet diameter to the maximum spreading width L_{max} and *We* for cylinder diameters of 2, 4, and 6 mm are shown in Figure 10(b). The normalized spreading ratio L_{max}/D_o was in line with $We^{1/4}$ for relatively large cylinder diameter and small *We*. Therefore, when the cylinder diameter is large, the estimated error of ϕ_e will be small. Conversely, when the diameter of the cylinder is small, the difference between L_{max} and D_{max}, which is caused by the shape of the droplet edge, becomes relatively large when it is converted to ϕ_e. As a result, it is considered that the droplet rebound condition is underestimated.

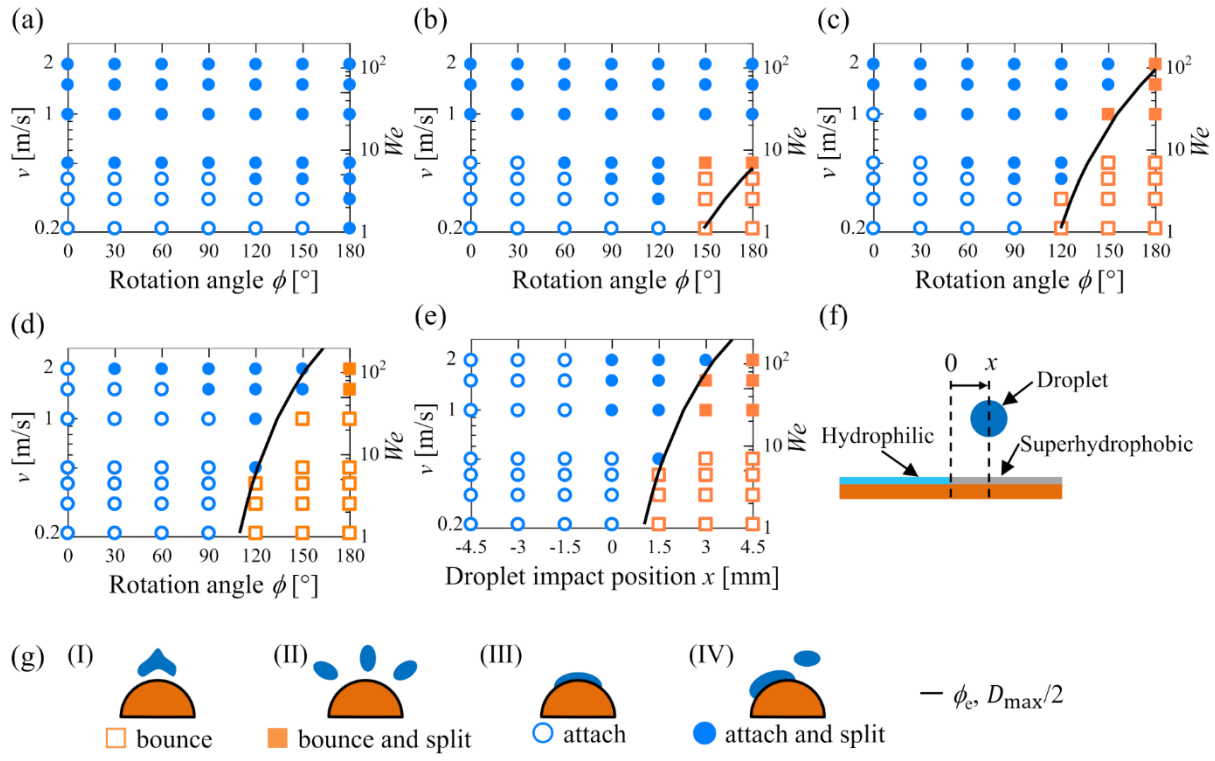

Figure 8. Phase diagrams of the droplet behavior after impact on the cylinder and the flat substrate as a function of *We* and the rotation angle ϕ for cylinder diameters of (a) 1 mm, (b) 2 mm, (c) 4 mm and (d) 6 mm, and behavior on the flat substrate as a function of *We* and the off-center distance for (e) flat substrate. (f)Schematic of the definition of impact position for the flat substrate. (g) Illustration of each phase.

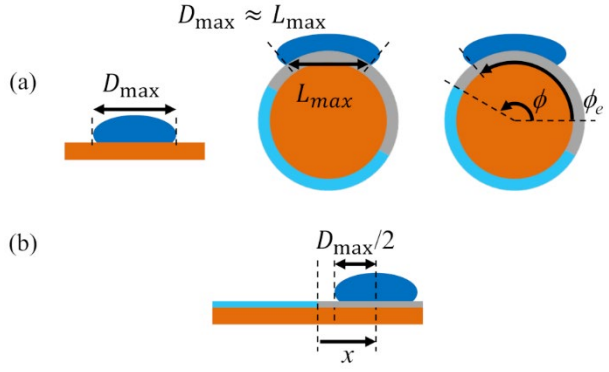

Figure 9. (a) Conversion of the maximum spreading width on the flat substrate to the cylinder angular

direction. (b) Maximum spreading width and impact position at the flat substrate.

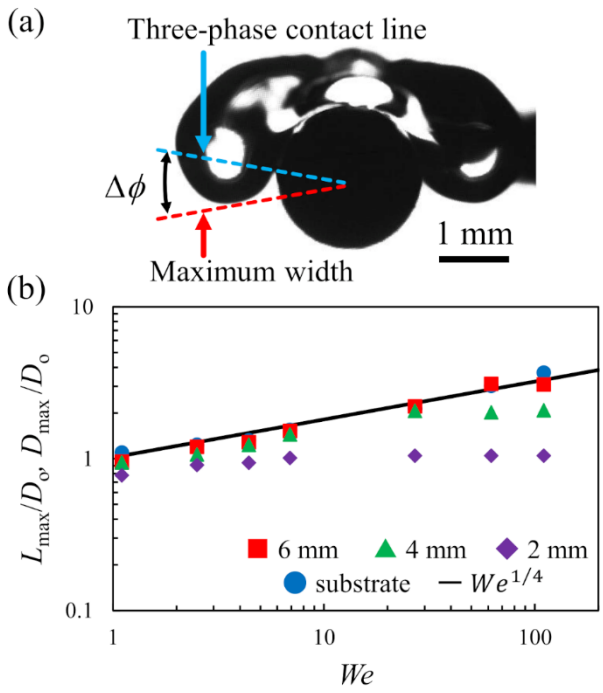

Figure 10. (a) Example of the difference between the maximum spreading width and three-phase contact line. (b) Relationship between *We* and the maximum spreading width.

CONCLUSIONS

We have conducted droplet impact experiments on cylinders with a wettability difference and estimated the impact behavior based on the maximum spreading width of the droplet. Copper cylinders with a wettability difference from hydrophilic to superhydrophobic in the circumferential direction were fabricated. Experiments were conducted with droplets of 2 mm in diameter, cylinder diameters ranged from 1 to 6 mm, and impact velocities ranged from 0.2 to 2.0 m/s.

Typical behavior after droplet impact was found that the droplet attached to the cylinder at rotation angles $\phi = 0°–60°$, bounced off the cylinder at $\phi = 120°–180°$, and moved to the hydrophilic

side of the cylinder at $\phi = 90°$ owing to the wettability difference for $D_c = 6$ mm and $v = 0.5$ m/s. The detail analysis revealed that the behavior of the droplets after impact was classified into four categories: the droplet attached to the surface, the droplet attached to the surface and split, the droplet bounced off the surface, and the droplet bounced off the surface and split. At high impact velocities, and for small D_c with low impact velocities, the droplet tended to split owing to its large inertia energy. In addition, the maximum width of the droplet was estimated from the Weber number and droplet diameter, which was converted to the counterclockwise angle from the horizontal axis ϕ_e to estimate the position of the left-hand side of the impacted droplet on the cylinder. The estimated threshold showed agreement with the experimental results for D_c =4, 6 mm and the flat substrate.

The results of the present study show new possibilities for controlling droplet impact behavior on cylindrical surfaces. This technique could be applied for ice prevention and self-cleaning surfaces. However, several challenges remain in this research. The investigation of discrepancies between predictions and experimental results at high velocity and small cylinder diameters conditions are needed for further accurate understanding of the impact behavior on curved surfaces with wettability difference. In addition, analysis of the size and number of splitting droplets after impact would also be needed.

ASSOCIATED CONTENT

Supporting Information

More detailed information about recording the movies of the droplet impact behavior on the cylinders

and movies of a droplet impacting the copper cylinder for v = 0.5 m/s, D_c = 6 mm, and ϕ = 0° (Movie 1), v = 0.5 m/s, D_c = 6 mm, and ϕ = 90° (Movie 2), v = 0.5 m/s, D_c = 6 mm, and ϕ = 180° (Movie 3), v = 0.2 m/s, D_c = 6 mm, and ϕ = 90° (Movie 4), v = 1.5 m/s, D_c = 6 mm, and ϕ = 90° (Movie 5), v = 0.5 m/s, D_c = 1 mm, and ϕ = 90° (Movie 6), v = 0.5 m/s, D_c = 2 mm, and ϕ = 90° (Movie 7), and v = 0.5 m/s, D_c = 4 mm, and ϕ = 90° (Movie 8). All of the videos are played back at 1/250× speed.

AUTHOR INFORMATION

*Corresponding author

Yutaka Yamada

Tel.: +81 86 251 8046. E-mail: y.yamada@okayama-u.ac.jp

ORCID

Yutaka Yamada: 0000-0002-2823-6790

Kazuma Isobe: 0000-0002-8621-5015

Notes

The authors declare no competing financial interest.

ACKNOWLEDGMENTS

This work was partly supported by the Kurita Water and Environmental Foundation (Grant No. 22K014), Japan. We thank Edanz (https://jp.edanz.com/ac) for editing a draft of this manuscript.

References

[1] Singh, M.; Haverinen, H. M.; Dhagat, P.; Jabbour, G.E. Inkjet Printing—Process and Its Applications. Adv. Mater. 2010, 22, 673-685

[2] Srikar, R.; Gambaryan-Roisman, T.; Steffes, C.; Stephan, P.; Tropea, C.; Yarin, A.L. Nanofiber coating of surfaces for intensification of drop or spray impact cooling. Int. J. Heat Mass Transf. 2009, 52, 5814–5826

[3] Maitra, T.; Antonini, C.; Tiwari, M. K.; Mularczyk, A.; Imeri, Z.; Schoch, P.; Poulikakos, D. Supercooled Water Drops Impacting Superhydrophobic Textures. Langmuir 2014, 30, 10855−10861

[4] Mishchenko, L.; Hatton, B.; Bahadur, V.; Taylor, J. A.; Krupenkin, T.; Aizenberg, J. Design of Ice-free Nanostructured Surfaces Based on Repulsion of Impacting Water Droplets. ACS Nano. 2010 4, 12, 7699-7707

[5] Bhushan, B.; Jung, Y. C.; Koch, K. Self-Cleaning Efficiency of Artificial Superhydrophobic Surfaces. Langmuir 2009, 25, 3240-3248

[6] Khojasteh, D.; Kazerooni, M.; Salarian, S.; and Kamali, R.; Droplet impact on superhydrophobic surfaces: A review of recent developments. J Ind Eng Chem 2016, 42, 1–14

[7] Han, X.; Li, J.; Tang, X.; Li, W.; Zhao, H.; Yang, L.; Wang. L. Droplet Bouncing: Fundamentals, Regulations, and Applications. Small 2022, 18, 2200277

[8] Zhang, B.; Sanjay, V.; Shi, S.; Zhao, Y.; Lv, C.; Feng, X.; Lohse, D. Impact Forces of Water Drops Falling on Superhydrophobic Surfaces. Phys. Rev. Lett. 2022, 129, 104501

[9] Josserand, C.; Thoroddsen, S.T. Annu. Rev. Drop Impact on a Solid Surface. Fluid Mech 2016, 48, 365–391

[10] Yarin, A.L. Drop Impact Dynamics: Splashing, Spreading, Receding, Bouncing... Annu. Rev. Fluid Mech 2006, 38, 159–192

[11] Pasandideh-Fard, M.; Chandra, S.; Mostaghimi, J. A three-dimensional model of droplet impact and solidification. Int. J. Heat Mass Transf. 2002, 45, 2229–2242

[12] Eggers, J.; Fontelos, M.A.; Josserand, C.; Zaleski, S. Drop dynamics after impact on a solid wall: Theory and simulations. Phys. Fluids 2010, 22, 062101

[13] Gunjal, P.R.; Ranade, V.V.; Chaudhari, R.V. Dynamics of Drop Impact on Solid Surface: Experiments and VOF Simulations. AIChE J 2005, 51, 1

[14] Cheng, X.; Sun, T.; Gordillo, L. Drop Impact Dynamics: Impact Force and Stress Distributions. Annu. Rev. Fluid Mech. 2022. 54, 57–81

[15] Du, J.; Wang, X.; Li, Y.; Min, Q.; Wu, X. Analytical Consideration for the Maximum Spreading Factor of Liquid Droplet Impact on a Smooth Solid Surface. Langmuir 2021, 37, 7582−7590

[16] Liu, Q.; Hau, J.; Lo, Y.; Li, Y.; Liu, Y.; Zhao, J.; Xu, L. The role of drop shape in impact and splash. Nat. Commun. 2021, 12, 3068

[17] Wang, F.; Fang, T. Retraction dynamics of water droplets after impacting upon solid surfaces from hydrophilic to superhydrophobic. Phys. Rev. Fluids 2020, 5, 033604

[18] Wang, Y.; Wang, Y.; Gao, S.; Yang, Y.; Wang, X.; Chen, M. Universal Model for the Maximum Spreading Factor of Impacting Nanodroplets: From Hydrophilic to Hydrophobic Surfaces. Langmuir

2020, 36, 9306−9316

[19] Liu, Y.; Whyman, G.; Bormashenko, E.; Hao, C.; Wang, Z. Controlling drop bouncing using surfaces with gradient features. Appl. Phys. Lett. 2015, 107, 051604

[20] Yun, S. Enhancing the Asymmetry of Bouncing Ellipsoidal Drops on Curved Surfaces. Langmuir 2020, 36, 14864-14871

[21] Chen, X.; Zhang, L.; Wang, Y.; Jin, J.; Wang, Y.; Yang, Y.; Gao, S.; Zheng, S.; Wang, X.; Lee, D. Effect of Asymmetry on the Contact Time of Droplet Impact on Superhydrophobic Cylindrical Surfaces. Langmuir 2023, 39, 19037−19047

[22] Chantelot, P.; Moqaddam, A.; Gauthier, A.; Chikatamarla, S.S.; Clanet, C.; Karlinc, I.V.; Quere, D. Water ring-bouncing on repellent singularities. Soft Matter 2018, 14, 2227.

[23] Jowkar, S.; Morad, M.R. Rebounding suppression of droplet impact on hot surfaces: effect of surface temperature and concaveness. Soft Matter 2019, 15, 1017−1026

[24] Chen, X.; Wang, Y.; Yang, Y.; Wang, X.; Lee, D. Contact Time of Droplet Impact on Superhydrophobic Cylindrical Surfaces with a Ridge. Langmuir 2023, 39, 18644−18653

[25] Liu, Y.; Andrew, M.; Li, J.; Yeomans, J.M.; Wang, Z. Symmetry breaking in drop bouncing on curved surfaces. Nat. Commun. 2015, 6, 10034

[26] Andrew, M.; Liu, Y.; Yeomans, J.M. Variation of the Contact Time of Droplets Bouncing on Cylindrical Ridges with Ridge Size. Langmuir 2017, 33, 7583−7587

[27] Yin, S.; Huang, Y.; Li, H.; Jia, P.; Fok, Y.; Peng, H.; Wong, T.N. Compound Droplet Impact on a Thin Hydrophobic Cylinder. Langmuir 2023, 39, 14758−14763

[28] Yamada, Y.; Isobe, K.; Horibe, A. Droplet motion on a wrinkled PDMS surface with a gradient structural length scale shorter than the droplet diameter. RSC Adv. 2022, 12, 13917–13923

[29] Wang, L.; Peng, B.; Su, Z. Tunable Wettability and Rewritable Wettability Gradient from Superhydrophilicity to Superhydrophobicity. Langmuir 2010, 26, 14, 12203–12208

[30] Wu, J.; Yin, K.; Xiao, S.; Wu, Z.; Zhu, Z.; Duan, J.; He, J. Laser Fabrication of Bioinspired Gradient Surfaces for Wettability Applications. Adv. Mater. Interfaces 2021, 8, 2001610

[31] Liu, C.; Sun, J.; Li, J.; Xiang, C.; Che, L.; Wang, Z.; Zhou, X. Long-range spontaneous droplet self-propulsion on wettability gradient surfaces. Sci. Rep. 2017, 7, 7752

[32] Xu, C.; Jia, Z.; Lian, X. Wetting and adhesion energy of droplets on wettability gradient surfaces. J. Mater. Sci. 2020, 55, 8185–8198

[33] Subramanian, R.S.; Moumen, N.; McLaughlin, J.B. Experiments on the Motion of Drops on a Horizontal Solid Surface Due to a Wettability Gradient. Langmuir 2006, 22, 2682-2690

[34] Chu, F.; Luo, J.; Hao, C.; Zhang, J.; Wu, X.; Wen, D. Directional Transportation of Impacting Droplets on Wettability Controlled Surfaces. Langmuir 2020, 36, 5855−5862

[35] Huang, J.; Wang, L.; He, K. Three-dimensional study of double droplets impact on a wettability-patterned surface. Comput. Fluids. 2022, 248 105669

[36] Cheng, Z.; Hou, R.; Du, Y.; Lai, H.; Fu, K.; Zhang, N.; Sun, K. Designing Heterogeneous Chemical Composition on Hierarchical Structured Copper Substrates for the Fabrication of Superhydrophobic Surfaces with Controlled Adhesion. ACS Appl. Mater. Interfaces 2013, 5, 8753−8760

[37] Chaudhury, M.K.; Whitesides, G.M. How to Make Water Run Uphill. Science 1992, 256,

[38] Mao, T.; Kuhn, D.; Tran, H. Spread and Rebound of Liquid Droplets upon Impact on Flat Surfaces. AIChE J 1997, 43, 9, 2157-2384

[39] Clanet, C.; Beguin, C.; Richard, D.; Quere, D. Maximal deformation of an impacting drop. J. Fluid Mech 2004, 517, 199–208.

1 Table of content

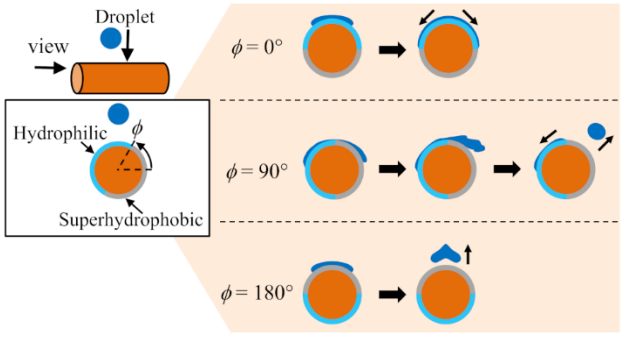

2

3

4